

# Geophysical Research Letters<sup>®</sup>

## RESEARCH LETTER

10.1029/2021GL094456

### Key Points:

- Mixing in a metal-rock mushy layer offers a promising mechanism to explain some geochemical observations linked to core-mantle interaction
- A mushy layer produced by core-mantle boundary topography may become weak and collapse due to gravity, enhancing mantle circulation
- Our models show that this “soft CMB” mechanism becomes dominant for viscosity contrasts of  $10^5$  or more, influencing deep mantle dynamics

### Supporting Information:

Supporting Information may be found in the online version of this article.

### Correspondence to:

K. W. Lim,  
[kangwei.lim@elsi.jp](mailto:kangwei.lim@elsi.jp)

### Citation:

Lim, K. W., Bonati, I., & Hernlund, J. W. (2021). A hybrid mechanism for enhanced core-mantle boundary chemical interaction. *Geophysical Research Letters*, 48, e2021GL094456. <https://doi.org/10.1029/2021GL094456>

Received 2 JUN 2021  
Accepted 8 NOV 2021

## A Hybrid Mechanism for Enhanced Core-Mantle Boundary Chemical Interaction

Kang Wei Lim<sup>1</sup> , Irene Bonati<sup>1</sup> , and John W. Hernlund<sup>1</sup> 

<sup>1</sup>Earth-Life Science Institute, Tokyo Institute of Technology, Meguro, Japan

**Abstract** Detection of chemical signatures from the core-mantle boundary (CMB) could provide an unprecedented glimpse into our planet’s deep interior and ancient past. Several isotopic and elemental anomalies in ocean island basalts (OIBs) have been proposed as core tracers. However, the process(es) by which particular chemical signatures from the core are conveyed into the mantle remain uncertain. Here, we propose a hybrid mechanism that results from a collaborative feedback between dynamic topography, porous infiltration of liquid metal into submerged rock, gravitational collapse of weakened metal-silicate mush, and draw-down of additional rocks from above in the induced small-scale mantle circulation. Using a mantle convection model coupled to gravitational spreading of a thin layer, we show that induced mantle circulation due to the gravitational collapse of the layer becomes comparable to buoyancy-driven mantle flow when the viscosity of the mushy layer is reduced to values  $\sim 10^5$  times smaller than the overlying mantle.

**Plain Language Summary** The core and mantle may be able to exchange matter by the build up of inverted mountains and valleys at their boundary, and the erosion of this terrain driven by gravity can significantly enhance mantle circulation through this region, allowing metals and rocks to mix more extensively than previously thought.

### 1. Introduction

Anomalous chemical signatures detected in some lavas are hypothesized to bear evidence of chemical interactions between the core and mantle. The rough idea is that these lavas are produced by partial melting of silicate material that has been transported upward from the CMB to the shallow mantle by deep-seated upwelling currents. A variety of studies have reported isotopic and elemental anomalies, such as coupled  $^{186}\text{Os}/^{188}\text{Os}$  and  $^{187}\text{Os}/^{188}\text{Os}$  that might be explained by fractional crystallization of the core (Brandon & Walker, 2005; Walker, 2000), high  $^3\text{He}/^4\text{He}$  (Bouhifd et al., 2013), high Fe/Mn (Humayun et al., 2004), coupled low  $^{182}\text{W}/^{184}\text{W}$  and high  $^3\text{He}/^4\text{He}$  (Mundl-Petermeier et al., 2017), correlations between  $^{182}\text{W}/^{184}\text{W}$ ,  $^3\text{He}/^4\text{He}$ , and Fe/Mn (Rizo et al., 2019), “nebular-like” D/H ratios (Hallis et al., 2015; Wu et al., 2018), noble gases (mainly He, Ne, and Xe) (Mukhopadhyay, 2012; Vogt et al., 2021), among others. Several mechanisms have been discussed in regard to core-mantle interactions, including: expulsion and/or crystallization of solids from the core (Badro et al., 2016; Buffett et al., 2000; Helffrich et al., 2018; Hirose et al., 2017; Kellogg & King, 1993; O’Rourke & Stevenson, 2016), metal infiltration driven by capillary action (Poirier et al., 1998), poro-viscoelastic shear-induced entrainment (Petford et al., 2005), interaction with a basal magma ocean in the early Earth (Labrosse et al., 2007; Trønnes et al., 2019; Zhang et al., 2000), pressure-driven infiltration of metal into pore spaces at CMB dynamic topographic lows (Kanda & Stevenson, 2006), ingestion of  $\sim\mu\text{m}$ -scale metal blebs via morphological instabilities (Otsuka & Karato, 2012), grain boundary diffusion (Hayden & Watson, 2007), and thermo-diffusion through interconnected metal intruded into the mantle (Leshner et al., 2020).

Direct physical entrainment of core material into rising mantle plumes (Otsuka & Karato, 2012; Petford et al., 2005) may seem to be the most straightforward way to explain the isotopic observations. However, such an exchange may be limited by the high density and low viscosity of the liquid outer core. In fact, the absence of a correlated enhancement of siderophile element abundances in lavas bearing low  $^{182}\text{W}/^{184}\text{W}$  and high  $^3\text{He}/^4\text{He}$  is inconsistent with direct transport of metal upward into the mantle (Mundl-Petermeier et al., 2017) and imply that there is no significant net enhancement of siderophile elements transported from the core to the mantle in these particular samples. This latter constraint may only be reconciled if

metals and silicates are allowed to undergo chemical interaction in the CMB region, while the metals are left behind as the reacted silicates are subsequently borne upward to the shallow mantle (Mundl-Petermeier et al., 2020). In addition to implying the presence of core-mantle interactions, some isotope ratios, such as  $^{186}\text{Os}/^{188}\text{Os}$  and  $^{187}\text{Os}/^{188}\text{Os}$ , can provide constraints on the interaction age. For example, modeling suggests that the source of Hawaiian lavas contains materials that interacted with the core during the Hadean, while the source of Gorgona komatiites is consistent with a more recent interaction time ( $\sim 1.5$  Ga) (Humayun, 2011).

Although it was originally proposed as a mechanism for producing a high electrical conductivity layer that provides magnetic coupling of core and mantle angular momentum, intrusion of metal into pore spaces inside mantle rocks at CMB dynamic topography lows (Kanda & Stevenson, 2006) may satisfy these constraints. In order for this mechanism to work, liquid metal must “wet” grain boundaries in the rock (Mann et al., 2008; Takafuji et al., 2004) to allow both efficient intrusion and subsequent compaction and expulsion of metals back into the core as material is transported away from the topographic lows where immersion and mixing occurs. Such compaction at the CMB has been shown to be very efficient unless grain sizes are very small, of order  $10\ \mu\text{m}$  or less (Buffett et al., 2000). Owing to the small length scales involved, of order the grain size, chemical equilibration inside a metal-silicate “mush” may be expected to occur on time scales much shorter than mantle convection flows (Hernlund & McNamara, 2015). Because CMB dynamic topography of order  $\sim 1$  km is expected (Olson et al., 1987), consistent with seismological constraints (Sze & van der Hilst, 2003; Tanaka, 2010), mantle circulation may expose  $\sim 10^{21}$  kg of mantle to silicate-metal interaction every time the CMB is refreshed by mantle convection. While this is small in comparison to the total mass of the Earth’s mantle ( $4 \times 10^{24}$  kg), if the mantle side of the CMB is replaced  $\sim 100$  times over Earth’s history, then the cumulative amount of exposed mantle material rises to of order  $\sim 1\%$  of the silicate Earth, which may be sufficient to account for occasional observations of core flavors in surface lavas (Hernlund & McNamara, 2015).

In this paper, we investigate a scenario in which a metal-silicate “mush” layer is formed by metal intrusion at CMB topographic lows, permitting the mixing, equilibration, and subsequent unmixing of silicates and metals in a Kanda-Stevenson-like mushy layer at the CMB. We additionally consider the potential for weakening and lateral gravitational collapse of the layer, as well as its consequent feedbacks with mantle convection. In particular, we are interested in exploring the degree to which collapse of a mushy layer is able to alter mantle convection circulation in the CMB region and enhance the degree of interaction between core and mantle materials. Using a coupled model of mantle convection and layer collapse, we show that this hybrid “soft CMB” mechanism becomes effective as the viscosity of the metal mush layer is reduced to  $\sim 10^5$  times smaller than the viscosity of the deep mantle, for which a secondary circulation arises around CMB topographic lows and may begin to exert a strong influence on deep mantle dynamics.

## 2. The “Soft CMB” Mechanism

The CMB is depressed into the core in the vicinity of mantle downwelling flows as a consequence of deviatoric stresses derived from buoyancy-driven mantle convection. The expected dynamic topography at the CMB is of order  $\sim 1$  km (Olson et al., 1987). At CMB pressure-temperature conditions, a liquid iron-alloy is expected to “wet” solid grain boundaries and intrude between the grains to form an interconnected network (Mann et al., 2008; Takafuji et al., 2004). Combined with the excess fluid pressure head induced in topographic lows, this drives intrusion of metal upward into submerged basal mantle rock (Kanda & Stevenson, 2006). The amount of metal that may be ingested into the mushy region is limited to the disaggregation fraction since solids must maintain a continuous touching network in order to transmit a contrasting pressure gradient relative to liquid metal, and may only penetrate into the mantle by an amount similar to the magnitude of CMB topography (i.e.,  $\sim 1$  km).

A metal mush mixture formed in CMB topographic lows will be buoyant with respect to the underlying core, and may become rheologically weakened, thus raising the possibility of gravitational collapse. Lateral spreading of metal mush draws more mantle down from above to maintain the dynamic topography dictated by large-scale mantle convection (Figure 1a). By creating a nonlinear feedback in the system, such collapse enhances circulation of mantle rock into and through the mushy layer (Figure 1b). The combined

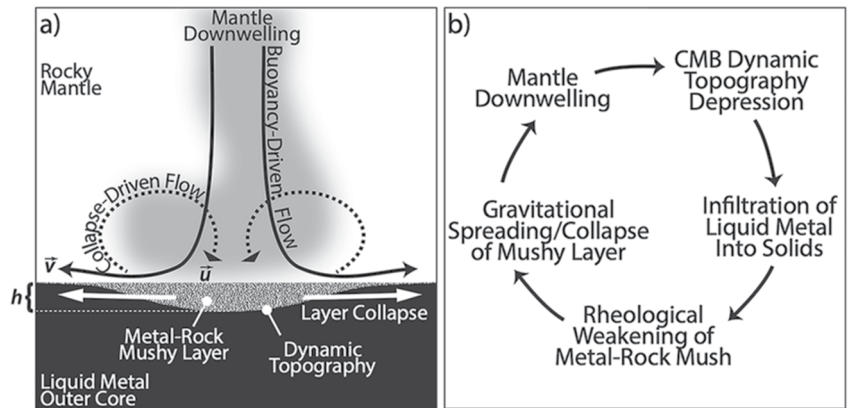


**Figure 1.** (a) Schematic illustration of the hybrid mechanism.  $h$  represents the thickness of the mushy layer, which is similar to the amplitude of dynamic topography. Black arrows illustrate downwelling mantle flow that induces dynamic topography. (b) Flow chart of the soft core-mantle boundary (CMB) mechanism explicitly showing the feedback loop.

effects result in a “softening” of the lower boundary condition for mantle convection in downwelling regions. As the metal mush spreads laterally and migrates away from mantle downwellings, the layer undergoes viscous compaction, squeezing liquid metal out from pore spaces that subsequently drains back into the liquid outer core. Efficient compaction in principle allows for rocks with core-like isotopic signatures to be transported to the surface without bearing excess siderophile elements (Ireland et al., 2011; Puchtel et al., 2005).

The “soft CMB” mechanism considered here is based on the action of dynamic topography, and may operate continuously throughout Earth’s history. However, dense (e.g., iron oxide-enriched) structures in the deep mantle may also depress into the core as the CMB analogue of “isostatic” topography (Hernlund & McNamara, 2015; Hernlund & Tackley, 2007; Lassak et al., 2010). Infiltration of metal and interaction in these kinds of dense rocky structures is also possible, and such materials may be sequestered over geologically long-time scales prior to upward entrainment by mantle convection into the shallow mantle. Dense chemical structures may be stirred by viscous coupling to larger scale mantle convection flows (Hernlund & Jellinek, 2010), leading to extensive mixing between metals and rocks over time. The situation may be even more complex, as deeply subducted lithospheric rocks that have chemically reacted with liquid metal in dynamic topography lows may become denser as a consequence, and as a result accumulate beneath upwelling regions. Other possibilities can include being entrained into other compositionally dense structures whose origin is distinct from core-mantle interaction. Even though the range of possibilities is very broad, such diversity may help explain the range of core-mantle interaction ages suggested by geochemical studies (Brandon et al., 2007; Mundl-Petermeier et al., 2019, 2020).

### 3. Model

Although the dynamics of mantle convection can be highly complex, here, we focus on building a basic illustrative model by assuming isoviscous mantle convection of an incompressible Boussinesq fluid in a Cartesian geometry. Normal stresses  $\sigma_{zz}$  exerted by the convective flows  $\vec{v}$  on the CMB raise a dynamic topography  $h$  given by

$$h(x, y) = \frac{\sigma_{zz}(x, y, z = 0)}{\Delta\rho g}, \quad (1)$$

where  $g$  is the acceleration of gravity and

$$\Delta\rho = \rho_m - \rho_{mix} = (1 - \phi)(\rho_m - \rho_r), \quad (2)$$

where  $\phi$  is the volume fraction of liquid metal (here it is assumed constant) intruded into the submerged portions of the metal-rock mush (i.e., where  $h < 0$ ), and  $\rho_m$  and  $\rho_r$  are the densities of liquid metal

( $\approx 9,900 \text{ kg m}^{-3}$ ) and mantle rock ( $\approx 5,500 \text{ kg m}^{-3}$ ), respectively. The quantity  $\rho_{\text{mix}}$  is the density of the mushy metal-rock mixture. We assume that only large-scale buoyancy forces from mantle convection are responsible for creating dynamic topography at the CMB.

The model is initiated from a quasi-steady convection solution with a downwelling in the middle of the domain and upwellings at the edges. We assume that decompaction and infiltration of metal into submerged rock occurs on time scales much shorter than the residence time of mantle rocks at the CMB. In other words, we assume that the vertical component of the Darcy velocity for upward metal percolation is large enough to keep up with the rate of mantle material being drawn down into the mushy region. This assumption can be written as

$$u_z^D(z=0) + v_z(z=0) = 0, \quad (3)$$

where  $u_z^D$  is the Darcy velocity and  $v_z$  is the mantle flow velocity just above the mushy layer.

In addition, the reverse process of compaction and expulsion of metal back to the core as the mush moves laterally away from depressions occurs on similarly short time scales. We expect variations in the mushy layer to occur over lateral length scales  $L$  that are much larger in comparison to  $h$ . In other words, since  $h/L \ll 1$ , we apply the “thin-layer approximation” from lubrication theory to describe gravitational collapse of the mushy layer (Hernlund & Bonati, 2019; Hier-Majumder & Revenaugh, 2010; Reynolds, 1886). Gravitational collapse of the mushy layer can be approximated as a diffusion process with

$$\frac{\partial h}{\partial t} = \frac{\Delta \rho g}{12\mu} \nabla_H^2 h^4, \quad (4)$$

where  $t$  is time,  $\mu$  is the (assumed constant) viscosity of the mushy layer, and  $\nabla_H^2$  is the horizontal Laplacian operator ( $\nabla_H^2 = \partial^2/\partial x^2 + \partial^2/\partial y^2$ ).

Mantle viscous forces are assumed to maintain the equilibrium dynamic topography described by Equation 1, keeping  $h$  constant for a given buoyancy-driven convection flow. Therefore, the effect of lateral spreading in the layer is to draw-down solid mantle from above to maintain the topography  $h$  that is dictated by the large-scale buoyancy-driven flow. We equate  $u_{z+} = (1 - \phi)\partial h/\partial t$ , where  $u_{z+}$  is the induced draw-down velocity of silicate solids from above at the top of the mushy layer. The factor  $(1 - \phi)$  accounts for the solid flux into the mushy region that is a mixture of both solids and metals. A secondary collapse-driven flow  $\bar{u}$  thus develops in the mantle that is coupled to gravitational spreading of the mushy layer described by the equation of  $u_{z+}$  at the lower boundary. With the assumption of a linear rheology, the collapse-driven Stokes flow  $\bar{u}$  can be solved separately from buoyancy-driven convection  $\bar{v}$  at each time step, after which they are combined to obtain a total effective velocity  $\bar{v}_{\text{eff}} = \bar{v} + \bar{u}$  that is used to advect temperature in the mantle. See the Supporting Information S1 for more details and the full set of equations.

We neglect the small variations in boundary topography when solving for  $\bar{v}$ , for which we assume free-slip (i.e., tangential stress-free) and impenetrable (i.e.,  $v_z(x, y, z=0) = 0$ ) boundary conditions at the CMB. However, we will need to obtain an estimate of the vertical velocity due to buoyancy-driven flow by itself (independently of collapse-driven flow) at the top of the layer, for which we use

$$v_{z+} \approx (1 - \phi) \frac{\partial v_z}{\partial z} \Big|_{z=0} h, \quad (5)$$

where the same  $\partial v_z/\partial z$  is used to compute  $h$  in Equation 1. This will be used to measure the relative contributions of solid flux through the metal-rock mush due to buoyancy-driven convection in order to compare it to collapse-driven flux.

The above assumptions are made in the context of considering the onset of small-scale collapse-driven flow as the viscosity of the mushy layer is reduced from ambient mantle values. However, these assumptions may not be suitable for the more general case in which the viscosity of the mush is even smaller, a topic that we will revisit in the discussion.

#### 4. Results

We solved for mantle convection flow in 2D Cartesian geometry with a Rayleigh number

$$Ra = \frac{\rho_r g \alpha \Delta T H^3}{\eta \kappa}, \quad (6)$$

for  $Ra = 10^4 - 10^6$ , where  $\alpha$  is the thermal expansivity,  $\Delta T$  is the super-adiabatic temperature change across the mantle,  $H$  is the mantle thickness,  $\eta$  is the reference viscosity of the mantle, and  $\kappa$  is the thermal diffusivity. We vary  $Ra$  by changing  $\eta$  while holding other quantities constant. The values used for the parameters are described in Table S1 in Supporting Information S1. Two different viscosity contrasts  $\xi = \mu/\eta$  are considered here:  $10^{-5}$  and  $10^{-6}$ . Larger values (i.e., higher mushy layer viscosities) do not yield any significant collapse-driven flow. These ratios capture the behavior at the point where collapse-driven flux through the mushy layer becomes comparable in magnitude to buoyancy-driven flux due to large-scale convection.

The temperature field, mushy layer thickness, and streamlines for both buoyancy-driven flow  $\Psi_v$  and flow due to the gravitational collapse of the mushy layer  $\Psi_u$  for  $Ra = 10^4$  and  $\xi = 10^{-6}$  are shown in Figures 2a–2d, respectively. The buoyancy-driven flow follows typical convective flow patterns, whereas for the collapse-driven flow, we observe a secondary circulation pattern in the vicinity of the downwelling just above the CMB. The secondary circulation arises from gravitational collapse of the mushy layer and we can see from the streamlines (Figure 2d) that downwelling flows are indeed enhanced, especially close to the CMB.

The pattern of  $\bar{u}$  and  $\bar{v}$  (Figures 2c and 2d) do not change significantly over the parameter ranges considered here. However, their amplitudes are sensitive to the input parameters. This leads to an enhancement of solid flux through the mushy layer that can be quantified as a “gain”  $G$  defined as

$$G = \frac{F_{cd}}{F_{bd}} = \frac{\int_S \frac{\rho_r}{2} (|u_{z+}| - u_{z+}) dS}{\int_S \frac{\rho_r}{2} (|v_{z+}| - v_{z+}) dS}, \quad (7)$$

where  $F_{cd}$  and  $F_{bd}$  are the mass fluxes due to the collapse-driven and buoyancy-driven flows, respectively, and  $S$  is the mantle-mushy layer interface. A plot of  $G$  as a function of  $Ra$  for two viscosity ratios is shown in Figure 3. The gain decreases moderately as  $Ra$  increases, while an order of magnitude decrease in  $\xi$  leads to an order of magnitude increase in  $G$ .

#### 5. Discussion

The models show that collapse-driven flux reaches parity with buoyancy-driven flux through the mushy layer for  $\xi \sim 10^{-5}$ . As shown in Figure 3, there is a modest decrease in  $G$  with increasing  $Ra$ , such that this basic conclusion is unlikely to change significantly (at the order of magnitude level) even allowing for broad uncertainties in lowermost mantle properties.  $G$  decreases with  $Ra$  because mantle viscosity ( $\eta$ ) is used as the control variable for convective vigor, thus a reduction in viscosity (increase in  $Ra$ ) decreases the magnitude of deviatoric stresses acting on the CMB topography more so than flow velocities increase with  $Ra$  ( $v \propto Ra^{2/3}$ ). This reduction in topography has a strong effect on gravitational collapse due to the nonlinear dependence upon  $h^4$  in the diffusion operator of Equation 4. The value of  $\xi$  is also an important variable that determines which type of flow dominates the system. We can scale the flux of each flow-type according to the velocities near the CMB as such:  $u \sim \Delta \rho g h^4 / (\mu L^2)$  and  $v \sim \delta \rho g H h / \eta$  where  $\delta \rho$  is the density variation caused by buoyancy forces inside the mantle. Comparing the two velocities gives

$$G \propto \frac{u}{v} \sim \left( \frac{\Delta \rho}{\delta \rho} \right) \left( \frac{h^3}{H L^2} \right) \left( \frac{1}{\xi} \right). \quad (8)$$

From Equation 1, we obtain a scaling for  $h$  according to the densities as follows:  $h/H \sim \delta \rho / \Delta \rho$ . This is plugged back into Equation 8 to eliminate the density ratio and  $H$  which finally gives the following scaling for  $G$

$$G \sim \left( \frac{h}{L} \right)^2 \left( \frac{1}{\xi} \right). \quad (9)$$

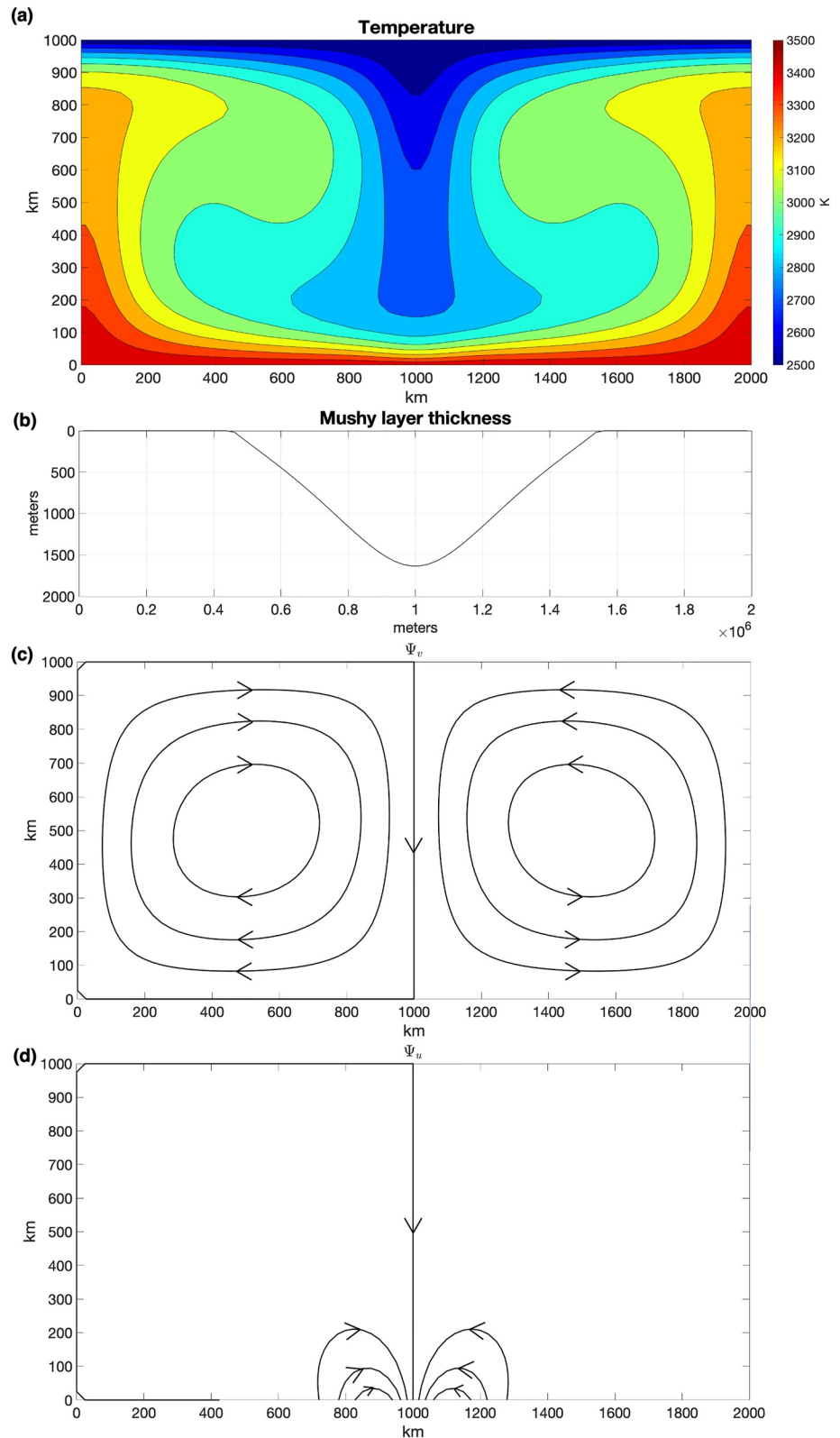


**Figure 2.** Results for  $Ra = 10^4$  and  $\xi = 10^{-6}$  at steady state. (a) Temperature field. (b) Mushy layer profile and thickness induced by deviatoric stresses at the core-mantle boundary (CMB). (c) Streamlines of buoyancy-driven flow with black arrows indicating the direction of the flow. (d) Streamlines of collapse-driven flow at the CMB with black arrows indicating the direction of the flow.

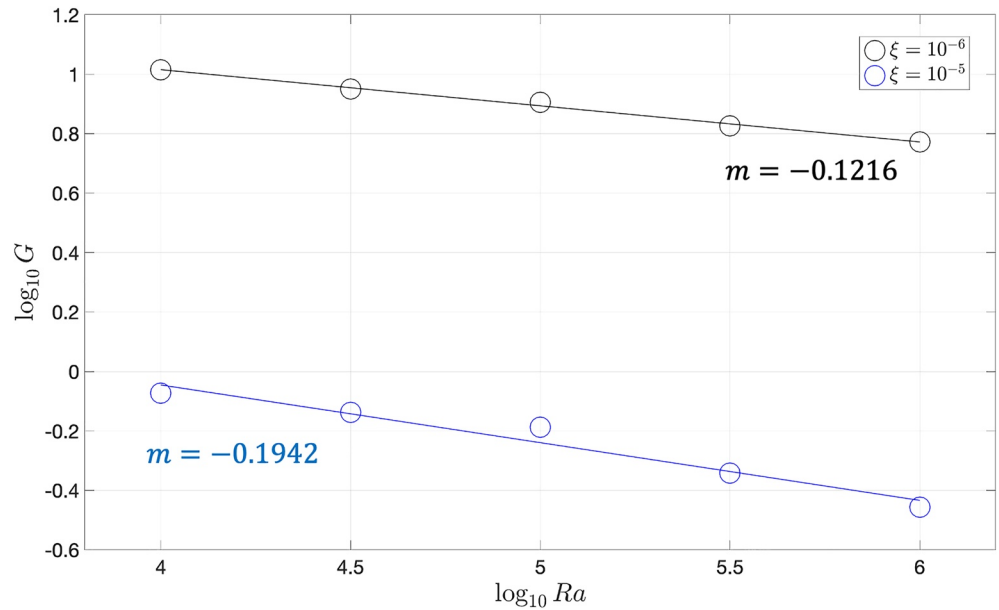


**Figure 3.** Plot of  $G$  against  $Ra$  in log scale. Lines show the least squares linear fit of  $\log_{10} G$  with  $\log_{10} Ra$ . The slope  $m$  represents the exponent in the following expression  $G \propto Ra^m$ . Black circles and blue circles correspond to  $\xi = 10^{-6}$  and  $\xi = 10^{-5}$  respectively.

Equation 9 tells us that the gain depends largely on the aspect ratio of the mushy layer and the viscosity contrast between the two domains. A preliminary estimate can be made to determine at which value of  $\xi$  the collapse-driven flow becomes dominant (i.e.,  $u/v \geq 1$ ) by estimating the order of magnitude for each term. Previously  $h$  was estimated to be  $\sim 10^3$  m, while in the numerical models,  $L \sim 10^6$  m. Combining these values together, we see that flow due to the collapse of the mushy layer becomes dominant when  $\xi \leq \sim 10^{-6}$ , in good agreement with our results. This implies that once the mushy layer becomes rheologically weak past a certain threshold, the positive feedback on the downwellings begins to dominate flows in the CMB region.

Figure 3 shows a clear negative trend between  $\log_{10} G$  and  $\log_{10} Ra$  that indicates a reduced enhancement of flow into the mushy layer with increasing convective strength of the mantle. In our calculations, the half-width at half the maximum amplitude of the layer was used to approximate the horizontal length scale  $L$ . From the numerical models, the mushy layer becomes smaller and narrower with increasing  $Ra$ . The following relations describing the dimensions of the mushy layer with  $Ra$  were obtained:  $h \sim HRa^{-0.2325}$  and  $L \sim HRa^{-0.1750}$  (see Figures S2a and S2c in Supporting Information S1). Plugging these values into Equation 9 shows that for a constant  $\xi$ ,  $G \sim Ra^{-0.1150}$ . This exponent is similar, though slightly larger, than what is obtained in our numerical models (Figure 3).

The efficacy of the soft CMB mechanism as measured by  $G$  dominantly depends on the viscosity ratio  $\xi$  between the metal mush and the solid mantle. The viscosity of the mush mixture is expected to decrease as metal fraction increases and drops to values similar to liquid metal above the disaggregation limit (when grains are no longer forming a continuous skeletal touching network). However, the ability for metal to intrude into the pore spaces depends on the existence of a grain-touching network and therefore this limit is never reached under the present assumptions. The key factor is the decrease in mixture viscosity  $\mu$  corresponding to the maximum infiltration capacity for the mush, at the point where it is no longer able to draw in additional metal. While a  $\xi$  of order  $10^{-5}$  or smaller is certainly plausible in this scenario, the grain scale dynamics of this process and the effects on mixture viscosity are complex and difficult to constrain, even within several orders of magnitude.

The model presented here is relatively simple and is intended to introduce the basic idea of the soft CMB mechanism. The assumptions behind our hybrid model may break down as the liquid fraction approaches the disaggregation limit and/or the viscosity of the mushy layer becomes very low (on the same order of magnitude as the liquid metal) or the liquid fraction in the mushy layer is greater than or equal to the

disaggregation limit. These can affect the model in two ways: (a) stresses from the gravitational collapse of the mushy layer become significant at the CMB and (b) the Darcy velocity in the layer is unable to keep up with the rate of mantle material being replenished by downwellings. When the viscosity of the mushy layer is greatly reduced compared to the overlying mantle, secondary flows due to the gravitational collapse of the mushy layer can become comparable or even greater than large-scale buoyancy-driven flows in the mantle, especially at the CMB. This implies that the vertical stresses creating dynamic topography will contain significant contributions from the collapse-driven component which was ignored in Equation 1.

As mushy layer viscosity decreases below values considered in this study, the assumption of Equation 3 may no longer be appropriate because upward liquid metal percolation needs to increase in proportion to the collapse-driven flow speed. The Darcy velocity of metal  $u_z^D$  may saturate at a maximum limiting value  $u_{z,\text{lim}}^D$ , and as a consequence liquid metal in the pore spaces will no longer be able to rise up quickly enough to match the downward flux of solid rock from above. In this situation, we expect that the top surface (i.e.,  $z = 0$ ) of the mushy layer will fall and the collapse-driven flow will weaken as the mushy layer becomes thinner. A new equilibrium may be reached if mantle downwelling decreases to  $|v_z| \approx |u_{z,\text{lim}}^D|$ , in which case the mushy layer will assume a new thickness given by

$$h_{\text{lim}} \approx \left( \frac{\Delta \rho g}{3\mu L^2 u_{z,\text{lim}}^D} \right)^{1/4}. \quad (10)$$

The details of the mushy layer dynamics at low viscosity and higher rates are likely to be more complex than considered here, and the scenario of a constant limiting Darcy velocity should be considered approximate.

Numerous other complications are expected to influence the efficacy of this mechanism. Variable viscosity, particularly temperature dependence, can have a strong influence on the lower boundary layer for mantle convection and needs to be considered in future studies. Furthermore, chemical reactions between rock and metal following exchange in a mush can change their densities and lead to enhanced convection and/or accumulation of layers on either side of the CMB, depending on whether reactions decrease or increase their densities. Finally, the long-time evolution with these and other effects also needs to be studied in greater detail, rather than simply considering a snapshot.

Seismological detection of metal-rock mushy regions caused by dynamic topography alone is challenging owing to the small ( $\sim 1$  km) thickness expected in this scenario. The mushy layer itself is not straightforwardly compatible with other kinds of features in the CMB region such as ultralow-velocity zones (ULVZ) or large low shear velocity provinces (LLSVP), which are one and two orders of magnitude thicker (respectively) than features considered in this scenario (Hernlund & McNamara, 2015). Use of high frequency peaceful nuclear explosion data to profile the CMB has revealed a thin slow layer that is compatible with the kind of mushy layer considered here (Ross et al., 2004), although this interpretation is not unique.

In summary, the soft CMB mechanism, whereby chemical interaction in a metal-rock mushy layer induced by CMB dynamic topography is enhanced by gravitational collapse, appears to be a viable mechanism for increasing core-mantle chemical exchange. Further study of this mechanism may generate new predictions that can be tested against seismological and other observations. The possibility that hybrid processes like these, which are produced by collaboration of simpler processes occurring across a broad range of scales, additionally serves to illustrate the capacity for nature to find degrees of freedom that often escape our attention.

### Data Availability Statement

The output data used to produce Figures 3, S2 and S3 in Supporting Information S1 can be accessed via the url: <https://doi.org/10.5281/zenodo.4892321>. The code used in the numerical models can be accessed via the url: <https://doi.org/10.5281/zenodo.4892344>.



### Acknowledgments

The authors wish to thank Ravi Kanda, Saswata Hier-Majumder, and Scott D. Hull for discussions, as well as Munir Humayun and David J. Stevenson for thoughtful reviews that helped improve the manuscript. Author KWL is financially supported by a scholarship from the Japanese Ministry of Education, Culture, Sports, Science and Technology (MEXT), IB by a graduate fellowship by the Japan Society for the Promotion of Science (JSPS), and JH was by JSPS Grant 19K04035.

### References

- Badro, J., Siebert, J., & Nimmo, F. (2016). An early geodynamo driven by exsolution of mantle components from Earth's core. *Nature*, *536*, 326–328. <https://doi.org/10.1038/nature18594>
- Bouhifd, M. A., Andrault, D., Bolfan-Casanova, N., Hammouda, T., & Devidal, J.-L. (2013). Metal-silicate partitioning of Pb and U: Effects of metal composition and oxygen fugacity. *Geochimica et Cosmochimica Acta*, *114*, 13–28. <https://doi.org/10.1016/j.gca.2013.03.034>
- Brandon, A., & Walker, R. (2005). The debate over core-mantle interaction. *Earth and Planetary Science Letters*, *232*, 211–225. <https://doi.org/10.1016/j.epsl.2005.01.034>
- Brandon, A. D., Graham, D. W., Waight, T., & Gautason, B. (2007). <sup>186</sup>Os and <sup>187</sup>Os enrichments and high-<sup>3</sup>He/<sup>4</sup>He sources in the Earth's mantle: Evidence from Icelandic picrites. *Geochimica et Cosmochimica Acta*, *71*(18), 4570–4591. <https://doi.org/10.1016/j.gca.2007.07.015>
- Buffett, B., Garnero, E., & Jeanloz, R. (2000). Sediments at the top of Earth's core. *Science*, *290*, 1338–1342. <https://doi.org/10.1126/science.290.5495.1338>
- Hallis, L. J., Huss, G. R., Nagashima, K., Taylor, G. J., Halldórsson, S. A., Hilton, D. R., et al. (2015). Evidence for primordial water in Earth's deep mantle. *Science*, *350*(6262), 795–797. <https://doi.org/10.1126/science.aac4834>
- Hayden, L. A., & Watson, E. B. (2007). A diffusion mechanism for core-mantle interaction. *Nature*, *450*(7170), 709–711. <https://doi.org/10.1038/nature06380>
- Helfrich, G., Ballmer, M. D., & Hirose, K. (2018). Core-exsolved SiO<sub>2</sub> dispersal in the Earth's mantle. *Journal of Geophysical Research: Solid Earth*, *123*, 176–188. <https://doi.org/10.1002/2017JB014865>
- Hernlund, J. W., & Bonati, I. (2019). Modeling ultralow velocity zones as a thin chemically distinct dense layer at the core-mantle boundary. *Journal of Geophysical Research: Solid Earth*, *124*, 7902–7917. <https://doi.org/10.1029/2018JB017218>
- Hernlund, J. W., & Jellinek, M. (2010). Dynamics and structure of a stirred partially molten ultralow-velocity zone. *Earth and Planetary Science Letters*, *296*, 1–8. <https://doi.org/10.1016/j.epsl.2010.04.027>
- Hernlund, J. W., & McNamara, A. K. (2015). 7.11—The core-mantle boundary region. In G. Schubert (Ed.), *Treatise on geophysics* (2nd ed., pp. 461–519). Elsevier. <https://doi.org/10.1016/B978-0-444-53802-4.00136-6>
- Hernlund, J. W., & Tackley, P. (2007). Some dynamical consequences of partial melting at the base of Earth's mantle. *Physics of the Earth and Planetary Interiors*, *162*, 149–163. <https://doi.org/10.1016/j.pepi.2007.04.005>
- Hier-Majumder, S., & Revenaugh, J. (2010). Relationship between the viscosity and topography of the ultralow-velocity zone near the core-mantle boundary. *Earth and Planetary Science Letters*, *299*(3), 382–386. <https://doi.org/10.1016/j.epsl.2010.09.018>
- Hirose, K., Morard, G., Sinmyo, R., Umemoto, K., Hernlund, J., Helfrich, G., & Labrosse, S. (2017). Crystallization of silicon dioxide and compositional evolution of the Earth's core. *Nature*, *543*(7643), 99–102. <https://doi.org/10.1038/nature21367>
- Humayun, M. (2011). A model for osmium isotopic evolution of metallic solids at the core-mantle boundary. *Geochemistry, Geophysics, Geosystems*, *12*, Q03007. <https://doi.org/10.1029/2010GC003281>
- Humayun, M., Qin, L., & Norman, M. (2004). Geochemical evidence for excess iron in the mantle beneath Hawaii. *Science*, *306*, 91. <https://doi.org/10.1126/science.1101050>
- Ireland, T., Walker, R., & Brandon, A. (2011). <sup>186</sup>Os–<sup>187</sup>Os systematics of Hawaiian picrites revisited: New insights into Os isotopic variations in ocean island basalts. *Geochimica et Cosmochimica Acta*, *75*(16), 4456–4475. <https://doi.org/10.1016/j.gca.2011.05.015>
- Kanda, R. V. S., & Stevenson, D. J. (2006). Suction mechanism for iron entrainment into the lower mantle. *Geophysical Research Letters*, *33*, L02310. <https://doi.org/10.1029/2005GL025009>
- Kellogg, L. H., & King, S. D. (1993). Effect of mantle plumes on the growth of D'' by reaction between the core and mantle. *Geophysical Research Letters*, *20*(5), 379–382. <https://doi.org/10.1029/93GL00045>
- Labrosse, S., Hernlund, J. W., & Coltice, N. (2007). A crystallizing dense magma ocean at the base of the Earth's mantle. *Nature*, *450*, 866–869. <https://doi.org/10.1038/nature06355>
- Lassak, T., McNamara, A., Garnero, E., & Zhong, S. (2010). Core-mantle boundary topography as a possible constraint on lower mantle chemistry and dynamics. *Earth and Planetary Science Letters*, *289*(1–2), 232–241. <https://doi.org/10.1016/j.epsl.2009.11.012>
- Leshner, C. E., Dannberg, J., Barfod, G. H., Bennett, N. R., Glessner, J. J., Lacks, D. J., & Brenan, J. M. (2020). Iron isotope fractionation at the core-mantle boundary by thermomodification. *Nature Geoscience*, *13*(5), 382–386. <https://doi.org/10.1038/s41561-020-0560-y>
- Mann, U., Frost, D. J., & Rubie, D. C. (2008). The wetting ability of Si-bearing liquid Fe-alloys in a solid silicate matrix—Percolation during core formation under reducing conditions? *Physics of the Earth and Planetary Interiors*, *167*(1), 1–7. <https://doi.org/10.1016/j.pepi.2007.12.002>
- Mukhopadhyay, S. (2012). Early differentiation and volatile accretion recorded in deep-mantle neon and xenon. *Nature*, *486*(7401), 101–104. <https://doi.org/10.1038/nature11141>
- Mundl-Petermeier, A., Touboul, M., Jackson, M., Day, J., Kurz, M., Lekic, V., & Walker, J. R. (2017). Tungsten-182 heterogeneity in modern ocean island basalts. *Science*, *356*, 66–69. <https://doi.org/10.1126/science.aal4179>
- Mundl-Petermeier, A., Walker, R., Fischer, R., Lekic, V., Jackson, M., & Kurz, M. (2020). Anomalous <sup>182</sup>W in high <sup>3</sup>He/<sup>4</sup>He ocean island basalts: Fingerprints of Earth's core? *Geochimica et Cosmochimica Acta*, *271*, 194–211. <https://doi.org/10.1016/j.gca.2019.12.020>
- Mundl-Petermeier, A., Walker, R., Jackson, M., Blichert-Toft, J., Kurz, M., & Halldórsson, S. A. (2019). Temporal evolution of primordial tungsten-182 and <sup>3</sup>He/<sup>4</sup>He signatures in the Iceland mantle plume. *Chemical Geology*, *525*, 245–259. <https://doi.org/10.1016/j.chemgeo.2019.07.026>
- Olson, P., Schubert, G., & Anderson, C. (1987). Plume formation in the D''-layer and the roughness of the core-mantle boundary. *Nature*, *327*(6121), 409–413. <https://doi.org/10.1038/327409a0>
- O'Rourke, J. G., & Stevenson, D. J. (2016). Powering Earth's dynamo with magnesium precipitation from the core. *Nature*, *529*(7586), 387–389.
- Otsuka, K., & Karato, S.-I. (2012). Deep penetration of molten iron into the mantle caused by a morphological instability. *Nature*, *492*(7428), 243–246. <https://doi.org/10.1038/nature11663>
- Petford, N., Yuen, D., Rushmer, T., Brodholt, J., & Stackhouse, S. (2005). Shear-induced material transfer across the core-mantle boundary aided by the post-perovskite phase transition. *Earth Planets and Space*, *57*(5), 459–464. <https://doi.org/10.1186/BF03351834>
- Poirier, J. P., Malavergne, V., & Le Mouél, J. L. (1998). Is there a thin electrically conducting layer at the base of the mantle? In *The core-mantle boundary region* (pp. 131–137). American Geophysical Union. <https://doi.org/10.1029/GD028p0131>
- Puchtel, I. S., Brandon, A. D., Humayun, M., & Walker, R. J. (2005). Evidence for the early differentiation of the core from Pt-Re-Os isotope systematics of 2.8-Ga komatiites. *Earth and Planetary Science Letters*, *237*(1–2), 118–134. <https://doi.org/10.1016/j.epsl.2005.04.023>
- Reynolds, O. (1886). IV. On the theory of lubrication and its application to Mr. Beauchamp tower's experiments, including an experimental determination of the viscosity of olive oil. *Philosophical Transactions of the Royal Society of London*, *177*, 157–234.

- Rizo, H., Andraut, D., Bennett, N., Humayun, M., Brandon, A., Vlastélic, I., & Murphy, D. (2019).  $^{182}\text{W}$  evidence for core-mantle interaction in the source of mantle plumes. *Geochemical Perspectives Letters*, 11, 6–11. <https://doi.org/10.7185/geochemlet.1917>
- Ross, A., Thybo, H., & Solodilov, L. (2004). Reflection seismic profiles of the core-mantle boundary. *Journal of Geophysical Research*, 109, B08303. <https://doi.org/10.1029/2003JB002515>
- Sze, E., & van der Hilst, R. (2003). Core mantle boundary topography from short period PcP, PKP, and PKKP data. *Physics of the Earth and Planetary Interiors*, 135(1), 27–46. [https://doi.org/10.1016/s0031-9201\(02\)00204-2](https://doi.org/10.1016/s0031-9201(02)00204-2)
- Takafuji, N., Hirose, K., Ono, S., Xu, F., Mitome, M., & Bando, Y. (2004). Segregation of core melts by permeable flow in the lower mantle. *Earth and Planetary Science Letters*, 224(3), 249–257. <https://doi.org/10.1016/j.epsl.2004.05.016>
- Tanaka, S. (2010). Constraints on the core-mantle boundary topography from P4KP-PcP differential travel times. *Journal of Geophysical Research*, 115, B04310. <https://doi.org/10.1029/2009JB006563>
- Trønnes, R., Baron, M., Eigenmann, K., Guren, M., Heyn, B., Løken, A., & Mohn, C. (2019). Core formation, mantle differentiation and core-mantle interaction within earth and the terrestrial planets. *Tectonophysics*, 760, 165–198. <https://doi.org/10.1016/j.tecto.2018.10.021>
- Vogt, M., Trieloff, M., Ott, U., Hopp, J., & Schwarz, W. H. (2021). Solar noble gases in an iron meteorite indicate terrestrial mantle signatures derive from Earth's core. *Communications Earth and Environment*, 2(1), 92. <https://doi.org/10.1038/s43247-021-00162-2>
- Walker, D. (2000). Core participation in mantle geochemistry: Geochemical Society Ingerson Lecture, GSA Denver, October 1999. *Geochimica et Cosmochimica Acta*, 64, 2897–2911. [https://doi.org/10.1016/s0016-7037\(00\)00429-4](https://doi.org/10.1016/s0016-7037(00)00429-4)
- Wu, J., Desch, S. J., Schaefer, L., Elkins-Tanton, L. T., Pahlevan, K., & Buseck, P. R. (2018). Origin of Earth's water: Chondritic inheritance plus nebular ingassing and storage of hydrogen in the core. *Journal of Geophysical Research: Planets*, 123, 2691–2712. <https://doi.org/10.1029/2018JE005698>
- Zhang, Z., Dorfman, S., Labidi, J., Zhang, S., Li, M., Manga, M., & Williams, Q. (2000). Primordial metallic melt in the deep mantle. *Geophysical Research Letters*, 43(8), 3693–3699. <https://doi.org/10.1002/2016GL068560>

## Reference From the Supporting Information

- Schubert, G., Turcotte, D. L., & Olson, P. (2001). *Mantle convection in the earth and planets*. Cambridge University Press. <https://doi.org/10.1017/CBO9780511612879>